

Slenderness Effects on the Flow Over an Array of Tall Buildings with Random Heights

Donnchadh MacGarry

Department of Aeronautics & Astronautics
University of Southampton
Boldrewood Campus, SO16 7QF, UK
dem1g18@soton.ac.uk

Zheng-Tong Xie

Department of Aeronautics & Astronautics
University of Southampton
Boldrewood Campus, SO16 7QF, UK
z.xie@soton.ac.uk

Christina Vanderwel

Department of Aeronautics & Astronautics
University of Southampton
Boldrewood Campus, SO16 7QF, UK
c.m.vanderwel@soton.ac.uk

ABSTRACT

The study in this report investigates the slenderness effects on the flow over a staggered array of random height buildings by adjusting the mean aspect ratio of the buildings. Large-Eddy Simulations was used to produce and gather data using both cyclic inlet-outlet and synthetic turbulence generation inlet boundary conditions. It was found that the slenderer buildings were less sensitive to the approaching wind direction. This was because the integral length scales of the turbulence generated by the slenderer buildings are significantly larger than for low-rise buildings.

1. INTRODUCTION

Many attempts have been made to use the logarithmic law equation to parameterise the flow for urban environments,

$$U = \frac{u_\tau}{\kappa} \ln \left(\frac{z-d}{z_0} \right) \quad (1)$$

where u_τ is the friction velocity, κ is the von Kármán constant, z_0 is the roughness length which is the height at which wind speed reaches zero and d is the zero-plane displacement which is a correction factor for the profile itself. It has been thought that building height h , packing density λ_p and frontal area λ_f were the most important variables. There have been studies exploring urban environments which have attempted to use these variables along with the log law equation to parameterise the flow (Grimmond & Oke, 1999), (Cheng & Castro, 2002). However, it has been found that these variables on their own are not enough to dictate the flow. Kanada, et al. (2013) found that the standard deviation of heights σ and the maximum building height h_{max} are also important parameters that influence the flow.

Further issues come to mind when it comes to the definitions of the variables, which had been given by Grimmond & Oke (1999). λ_f is the ratio of the frontal area A_F to the total lot area A_T . This latter term is relatively easy to define for a structured array of repeated buildings such as an aligned array or staggered array. However, it is not so easy to define A_T for buildings arranged in an unstructured manner, which is more often the case in real world situations. Grimmond & Oke used the solid area of the buildings in a crosswind section for their definition of A_F . However, it has

been suggested that using the projection area of the buildings in the streamwise direction would be a better way to define A_F . The most appropriate definition of A_F becomes even trickier to determine when different approaching wind directions are used.

This suggests the requirement of an additional variable to help parameterise the flow. This study focuses on the impact that the aspect ratio AR of the buildings has on the flow, with AR defined as the ratio of the building width to height, $AR = b/h$. Smaller values of AR occur for slenderer buildings, which are typical of high-rise buildings seen in large cities. AR is an easier term to define for an urban environment than λ_f , since it only depends on the building's dimensions and doesn't depend on the arrangement of the buildings, or the approaching wind direction.

2. GEOMETRY DESIGN & SIMULATION SETTINGS

A staggered array of cuboid buildings with random heights was chosen for the investigation that is shown in Figure 1a. It was based on the design from Cheng & Castro (2002), but on a full-scale size for the dimensions. A unit of the array contains sixteen buildings of square cross section. The buildings have a width of $b = 10\text{m}$ and a packing density of $\lambda_p = 0.25$. The heights of the buildings were distributed normally about a mean of $h_m = 10\text{m}$ with a standard deviation of $\sigma = 3\text{m}$, where $h_{max} = 17.2\text{m}$. This gave the array a mean aspect ratio of $AR = 1$.

Two different designs were used for the creation of the building array with a mean aspect ratio of $AR = 0.25$. The first design, shown in Figure 1b, increased the heights of the buildings by a factor of four giving them a $h_m = 40\text{m}$. The second design, which isn't pictured, fixed the heights of the buildings to maintain $h_m = 10\text{m}$, and instead reduced the horizontal length dimensions of the geometry by a factor of four so that $b = 2.5\text{m}$. These two $AR = 0.25$ building array designs are geometrically identical, being scale models of each other. It is important to stress that σ/h_m , h_{max}/h_m and

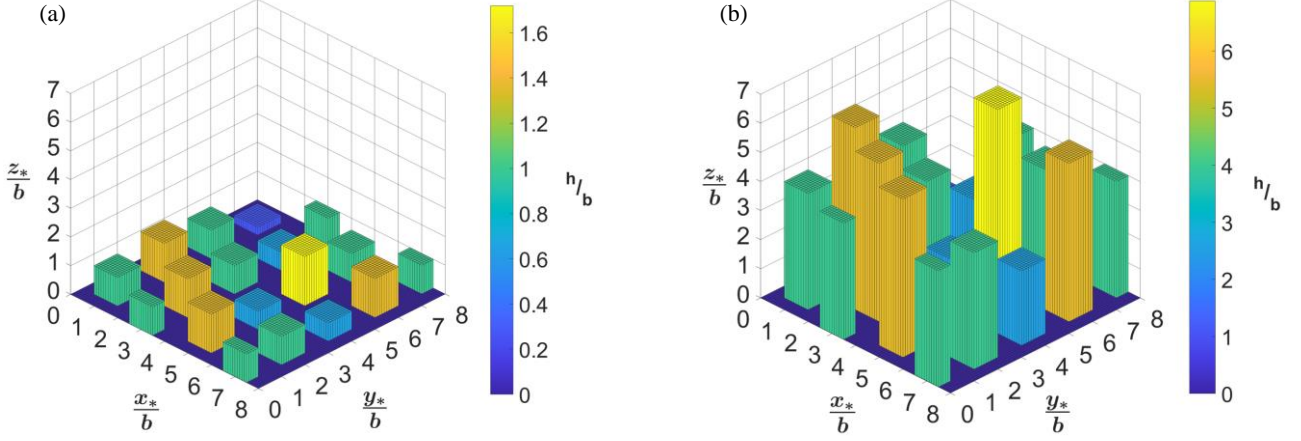


Figure 1: Building array designs. (a) $AR = 1$, $h_m = 10\text{m}$, $b = 10\text{m}$. (b) $AR = 0.25$, $h_m = 40\text{m}$, $b = 10\text{m}$.

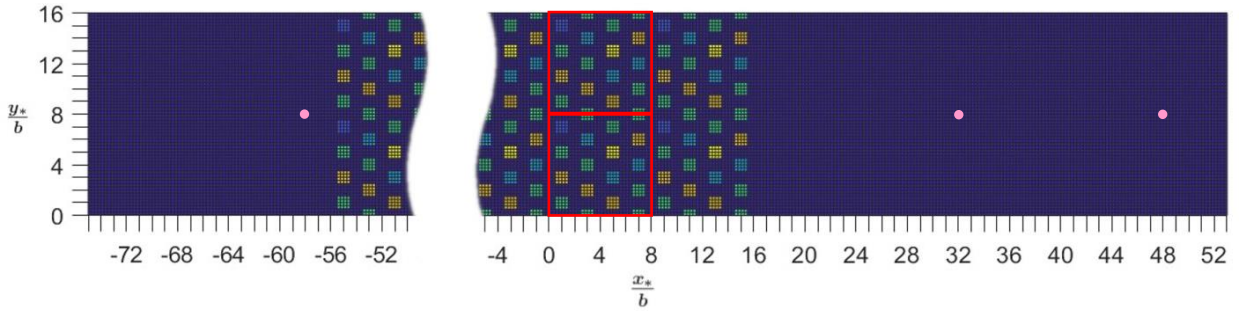


Figure 2: Domain used with the STG inlet boundary condition, not to scale. Units where spatial averaging was conducted outlined in red. Reference points for two-point correlation located at the pink dots.

λ_p for both $AR = 0.25$ building array designs are the same as that for the $AR = 1$ building array.

Large Eddy Simulations (LES) in PALM-4U (Maronga, et al., 2015) were conducted on parallel computation with up to 3200 cores. Cyclic boundary conditions were applied to the sidewalls of the domain, a Neumann stress free condition was applied to the domain ceiling and a Dirichlet no slip condition was applied to the domain ground and building surfaces. A third order Runge-Kutta method was used for the timestep scheme, which required the fifth order scheme of Wicker and Skamarock to be used for the advection scheme to maintain a stable numerical solution. The timestep scheme set the Courant number to a value of 0.9, where the timestep automatically adjusted to maintain this value.

Two inlet boundary conditions were tested in this study, each requiring a different domain design. A cyclic inlet-outlet boundary condition was used to emulate the flow over a large urban environment of the repeated building arrays, greater than the number that could be contained in a domain. The results for cyclic inlet-outlet are used to discuss slenderness effects on the flow quantities in Section 3 and the wind direction effects in Section 4. The other inlet boundary condition used a synthetic turbulence generated (STG) profile. This type of simulation was used to verify the results that the cyclic inlet-outlet simulations produced and provided a means for conducting the integral length scale analysis of the turbulence in the wake as seen in Section 5.

For the cyclic inlet-outlet boundary condition, the domain was composed of the unit array repeated in a 2×2 pattern and had a height of $H = 12h_m$. The driving force for the cyclic inlet-outlet boundary condition was created by a constant pressure gradient along the streamwise direction of the

approaching wind, with $dP/dx = -0.0002 \text{ Nm}^{-1}$. The constant pressure gradient was used to calculate the frictional velocity u_τ , along with the domain height and air density ρ (Xie, et al., 2008),

$$u_\tau = \sqrt{\frac{H}{\rho} \left| \frac{dP}{dx} \right|}. \quad (2)$$

Spatial averaging results for simulations with this design were calculated using the whole 2×2 unit domain.

The domain designed for the STG inlet, see Figure 2, contained the unit arrays repeated in a 9×2 pattern, which totalled 36 rows of buildings. As with the domain for the cyclic inlet, a domain height of $H = 12h_m$ was used. The distance from the inlet to the centreline of the first row of buildings was $20b$, while the distance from the centreline of the last row of buildings and outlet was $38b$. The STG profile used at the inlet was designed based off wind tunnel experimental data from Marucci, et al., (2018) and LES data from Sessa, et al., (2020). This inlet profile had turbulence length scales of $(4b, b, b)$ and a frictional velocity of $u_\tau = 0.067 \text{ ms}^{-1}$. Some modifications to the inlet profiles were made which is further discussed in Section 5.1. Spatial averaging was conducted over the two units that contained the buildings in rows 29-32 which are highlighted in Figure 2.

Wind direction effects were also considered, where approaching angles α of 0° , 22.5° , 45° , 67.5° and 90° were tested in the domain with the cyclic inlet-outlet boundary condition. This required two co-ordinate systems to be defined. The first system (x, y, z) corresponds to the

approaching wind's streamwise, spanwise and vertical directions. The second system (x_*, y_*, z_*) corresponds to the length, width and vertical components of the building geometry. The (x, y) and (x_*, y_*) axes were aligned only when $\alpha = 0^\circ$, whereas the z and z_* axes were always aligned since they are both along the vertical.

A cartesian mesh with a resolution of $b/10$ was used for all the simulations, ensuring consistency in the resolution across the buildings, maintaining consistency (Xie & Castro, 2006). The results from the cyclic inlet-outlet simulations using the $AR = 1$ buildings were verified against wind tunnel results from Cheng & Castro (2002), and LES results from Xie, et al. (2008). Despite a difference in Reynolds number with the

small-scale model from previous studies and the full-scale model being examined here, the non-dimensional profiles of the spatially averaged mean flow and turbulent quantities were in good agreement. This agreed with point made by Xie & Castro (2006), where flow over this geometry had a weak dependency on Reynolds number. Mesh independency was confirmed after similar results were produced when using a refined mesh resolution of $b/20$.

3. SLENDERNESS EFFECTS ON THE MEAN VELOCITY FIELD AND TURBULENT STRESSES

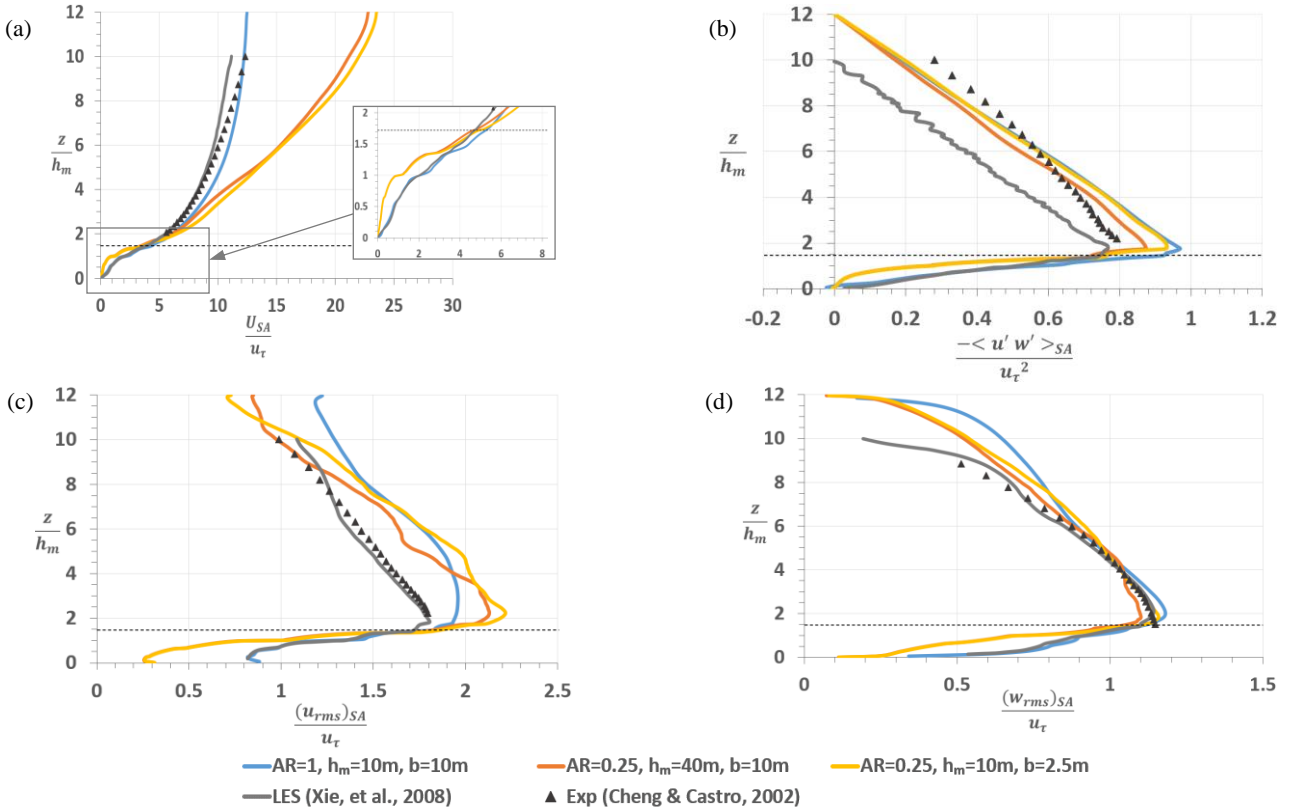


Figure 3: Profiles of the horizontally spatially averaged flow for a cyclic inlet-outlet, with wind approaching at an angle of $\alpha = 0^\circ$ (a) Mean streamwise velocity. (b) Shear stress. (c) Streamwise velocity fluctuations. (d) Vertical velocity fluctuations.

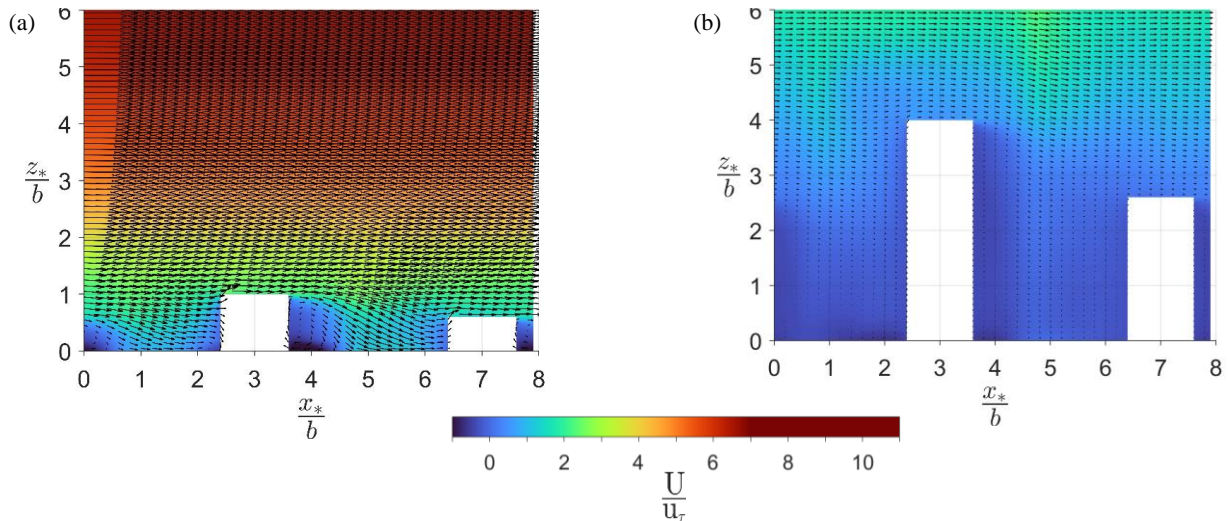


Figure 4: Mean velocity vector field along $y_* = 4b$, with wind approaching at an angle of $\alpha = 0^\circ$. (a) $AR = 1$. (b) $AR = 0.25$.

Near identical results were produced for the two different $AR = 0.25$ building array designs. This gives evidence that the flow is unchanged for geometrically identical building arrays, meaning that the changes seen to the flow in this study are purely due to the aspect ratio of the buildings, i.e., slenderness effects. For that reason, it is only necessary to refer the building array's aspect ratio for the remainder of this paper. The other dimensions such as building width and height do not need to be specified.

It was found that the horizontally spatially averaged velocity and turbulent quantities of the flow within the canopy layer, were smaller in magnitude for the $AR = 0.25$ building array than it was for the $AR = 1$ building array. This is shown in Figure 3a and 3b. This difference was most significant between the ground $z = 0$ and the mean building height $z = h_m$. Not all cases had the extrapolated values on the ground from the linear regime of the Reynolds shear stress collapsing to the expected value of unity (Eq. 2). This is due to small uncertainties of the Reynolds number, domain height and the existence of the building's solid volume.

Examining the mean velocity field on a vertical streamwise plane, such as the one in Figure 4 along $y_* = 4b$, can explain the reason for the change in the profiles of the velocity and turbulent quantities. The flow coming off top of the $AR = 1$ buildings, is mixed into the bottom of the canyon behind before reaching the next building downstream. This is known as a wake interference regime. The mixing allows for the flow throughout the canopy layer to become reenergised. On the other hand, the flow coming off the top of the $AR = 0.25$ buildings does not get mixed down towards the base of the next building downstream. Instead, a skimming regime occurs due to the heights of the buildings having increased relative to the spacing, which prevents much of the reenergising of the flow below the mean building height throughout the domain. The reduced mixing within the canopy layer for the slenderer buildings, decreases the ability to re-energise the flow within this region. It is the cause for the smaller magnitudes in the profiles of the spatially averaged velocity and turbulent quantities within the canopy layer for those buildings.

4. WIND DIRECTION EFFECTS

The interaction between wind direction effects and slenderness effects can also be observed in the spatially averaged mean velocity profiles of Figure 5. It is quite evident within the canopy layer, that the spread in the profiles is much larger for the $AR = 1$ building array than it is for the $AR = 0.25$ building array. Once more this is most notable below the mean building height. The same trend was also observed with the spatially averaged turbulent quantities, whose figures are not included in this report. The skimming regime flow that occurred for the $AR = 0.25$ buildings, is a one reason for the reduction in the spread of the spatially averaged flow profiles. Differences in the flow near the tops of the slenderer buildings due to the change in wind direction, are not going to impact the flow around the base of the buildings since there is not much mixing of the air between these two regions.

The horizontally spatially averaged flow angle β within the domain was calculated at different heights for each of the approaching wind directions. The difference between this flow angle and the approaching wind direction at these heights was plotted in Figure 6. Unsurprisingly for both sets of building arrays, the largest deflections are seen at lower heights due to the presence of more buildings in the horizontal slices that the

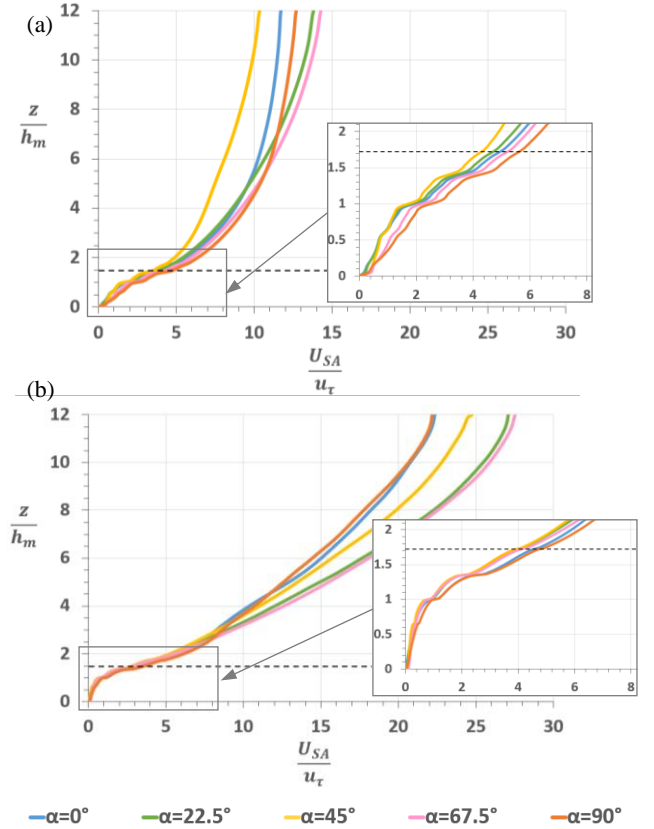


Figure 5: Spatially averaged mean streamwise velocity plots for different approaching wind directions angles α . (a) $AR = 1$. (b) $AR = 0.25$.

flow must navigate around. The $AR = 0.25$ buildings have less of an impact in deflecting the flow from its initial direction than the $AR = 1$ buildings do. It can be considered that due to the height dimension being significantly longer than cross-section length dimensions for the slenderer

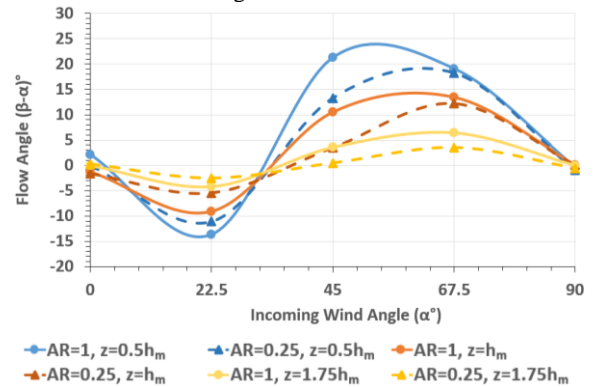


Figure 6: The variation of the horizontal spatially averaged flow angle β , for a range of incoming wind angles α at various heights.

buildings, the shape of the cross-section has less influence on the flow. The slenderer buildings act more like thin, cylindrical objects that are less sensitive to changes in the approaching wind direction. More quantitative analysis is carried out in Section 5. For this layout of random heights in the building array, the wind tends to favour being deflected in a positive direction once the approaching wind direction is above 30° .

5. SLENDERNESS EFFECTS ON THE INTEGRAL LENGTHSCALE IN THE WAKE

5.1 Comparison between periodic and synthetic turbulence inflow

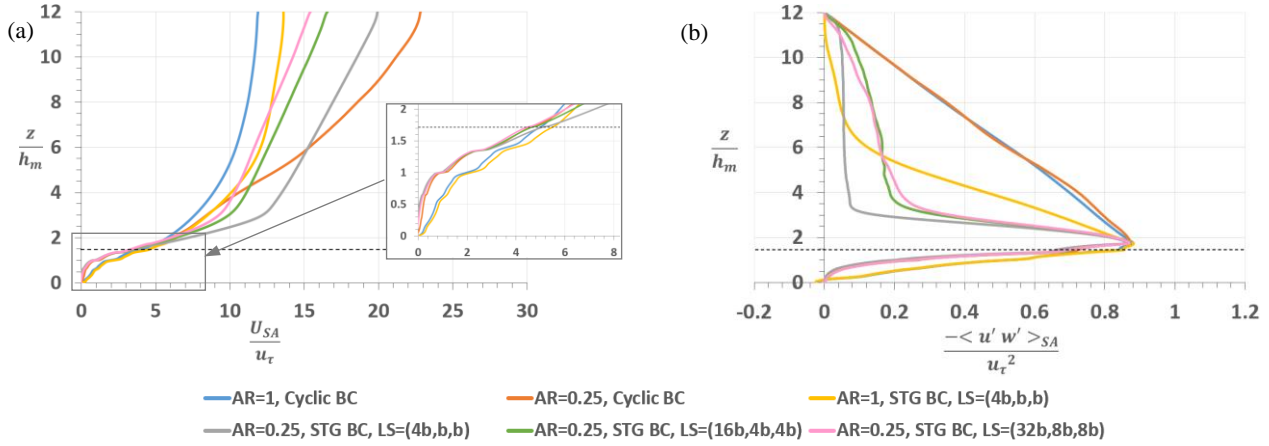


Figure 7: Comparison of the horizontally spatially averaged flow profiles for cyclic inlet and STG inlet simulations. (a) Streamwise mean velocity. (b) Shear stress.

Initial simulations using the STG profile at the inlet based on the data from Marucci, et al., (2018) and Sessa, et al., (2020) were conducted and compared with the cyclic case. Results, not pictured in this report, for the spatially averaged mean velocity and turbulent fluctuations with this inlet boundary condition agreed well with those for the cyclic boundary condition at heights within the canopy layer for both aspect ratios. For the $AR = 0.25$ building array, the spatially averaged mean velocity profile was also notably smaller in magnitude in the upper half of the domain compared to the cyclic case and the fluctuations decayed more rapidly above the canopy layer. The magnitude of the vertical shear stress profile decayed completely, indicating that the turbulence above the canopy layer was isotropic. This suggested that the current STG inlet boundary condition was not well suited to the $AR = 0.25$ buildings, as the building geometry was not able to sustain the inlet turbulence above the canopy layer.

Two modifications were made to the inlet boundary condition. The first created a new mean velocity profile at the inlet, by patching the original inlet's mean velocity profile within the canopy layer, to the spatially averaged mean velocity profile at the top of the domain for the cyclic inlet-outlet simulations which was larger in magnitude well above the canopy layer. This was done to test if a larger mean velocity was required to maintain the fluctuations in the flow. However, the change only had a limited impact on the turbulent quantities in the spatially averaged region for the STG inlet simulations. The second modification was to adjust the turbulence length scales used in the STG inlet for the $AR = 0.25$ buildings, where inlet length scales of $(16b, 4b, 4b)$ and $(32b, 8b, 8b)$ were tested.

To have a comparison with the cyclic case, the effective local u_τ for the STG cases needs to be estimated in the spatially averaged region. This is taken as the value on the ground extrapolated from the linear regime of the Reynolds shear stress in the same AR cyclic case, presented in Table 1. Figures 7a and 7b show the spatially averaged mean velocity and vertical shear stress profiles for the STG inlet simulations of both building aspect ratios along with the counterparts from the cyclic inlet-outlet simulations. As discussed in Section 3, not all cyclic inlet-outlet cases had the extrapolated values on

the ground from the linear regime of the Reynolds shear stress collapsing to the value of unity. To simplify the comparison, all the Reynolds shear stresses for the cyclic inlet-outlet cases were adjusted to have the extrapolated value on the ground to

be unity. The mean velocity and vertical shear stress profiles in Figures 7a and 7b have a strong alignment within the canopy layer for both the cyclic and synthetic simulations. The choice of length scale for the STG inlet simulations does not have a noticeable impact on the profiles within the canopy layer, which was also noted by Sessa, et al., (2020). The turbulence above the canopy layer has been better maintained when inlet length scales of $(16b, 4b, 4b)$ and $(32b, 8b, 8b)$ were used at the inlet for the $AR = 0.25$ buildings. Despite this their profiles are still quite decayed compared to that of the cyclic simulations. Increasing the number of repeated building units ahead of the spatial averaging region would allow the flow above the canopy layer to further develop and form a profile that would better match the cyclic simulations.

Table 1. Local u_τ in the spatially averaged region for the synthetic turbulence inlet boundary conditions.

AR=1, LS = (4b,b,b)	AR=0.25, LS = (4b,b,b)	AR=0.25, LS = (16b,4b,4b)	AR=0.25, LS = (32b,8b,8b)
0.079 ms ⁻¹	0.076 ms ⁻¹	0.092 ms ⁻¹	0.099 ms ⁻¹

5.2 Integral Length Scales in the Wake Flow

Time series data of the STG simulations was collected at various points. This report focuses on three reference points that are indicated by the pink dots in Figure 2. They lie along the centre span of the domain at the half-mean building height. One of these reference locations is before the buildings at $x = -58b$, and two are in the wake at $x = 32b$ and $x = 48b$.

The time series data was used to calculate the streamwise and spanwise two-point correlation coefficients of the streamwise velocity about the reference point. When possible, the correlation coefficients were averaged along the axis about either side of the reference point. Figure 8 contains the spanwise correlation coefficient plot about the reference point in the wake at $(48b, 8b, 0.5h_m)$. It is very evident that stronger positive correlation is maintained for longer distances from the reference point for the $AR = 0.25$ buildings. The same was

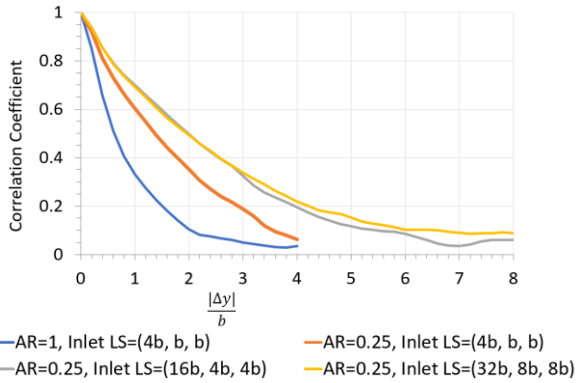


Figure 8: Two-point correlation coefficient of u in the spanwise direction about the reference point **(48b, 8b, 0.5h_m)**.

seen for the streamwise correlations which aren't pictured in this report. The correlations when using the inlet length scales of $(16b, 4b, 4b)$ and $(32b, 8b, 8b)$ are very similar in shape, indicating a convergence to a result that would be produced if more rows of buildings were added to the domain to allow the flow to develop further.

The two-point correlation coefficient profiles about the reference points were integrated to determine the integral length scales of the eddies, where a coefficient value of 0.1 was used as the cut-off point for the integration. The calculated values of the streamwise integral length scale L_x and spanwise integral length scales L_y at the reference positions, are presented in Table 2. In all cases the integral length scales for the $AR = 0.25$ buildings are substantially larger than those for the $AR = 1$ buildings. As with the two-point correlations, there is convergence in the integral length scales produced by the flow over $AR = 0.25$ buildings for the inlet length scales of $(16b, 4b, 4b)$ and $(32b, 8b, 8b)$. These length scales are closer in magnitude to each other than the equivalent integral length scale produced by the inlet length scale of $(4b, b, b)$. Eddies with length scales larger than that of the width of the building interact differently than eddies with length scales equal in size to the width of the building. This had been seen before in Section 4 with the wind direction effects. The slenderer buildings had been less sensitive to incoming wind direction due to interacting with larger eddies generating from buildings upstream than had been seen with the low-rise buildings.

Table 2. Streamwise (L_x) and spanwise (L_y) integral length scales at locations $(x, 8b, 0.5h_m)$. L_i , inlet length scales.

	AR=1, $L_i/b =$ (4,1,1)	AR=0.25, $L_i/b =$ (4,1,1)	AR=0.25, $L_i/b =$ (16,4,4)	AR=0.25, $L_i/b =$ (32,8,8)
L_x	32b	1.80b	-	5.74b
	48b	2.37b	5.83b	7.57b
	-58b	0.54b	0.56b	1.51b
L_y	32b	0.63b	1.01b	1.43b
	48b	0.75b	1.15b	1.59b

It had been stated that the integral length scales of the eddies in the wake of buildings can be approximated being the building's width (Castro, et al., 2006) as is done when using

an STG inlet with length scales of $(4b, b, b)$. However, for the slenderer buildings this isn't the case as has been shown here. The heights of the buildings must also be accounted for when trying to approximate these length scales, becoming increasingly significant the slenderer the building gets as the height dominates over the cross section.

CONCLUSIONS

Just as Xie & Castro (2006) had observed in their investigations of the building array created by Cheng & Castro (2002), the flow in this urban environment has little dependency on Reynolds number, due to the flow being dominated by the large scale eddies created by the separation along the sharp edges of the buildings. This was seen by the near-identical results produced by the two $AR = 0.25$ building array designs, despite wind flow settings not being scaled to maintain a consistent Reynolds number.

The change to the flow regime that were observed between the $AR = 1$ and $AR = 0.25$ building arrays, suggests that aspect ratio plays a significant role on the size of the eddies seen in the flow. The ability of the eddies to mix and re-energise the flow in the bottom region of the canopy layer, is impacted by the aspect ratio of the buildings in the array.

The slenderer $AR = 0.25$ building arrays were less sensitive to the oncoming wind direction. This was seen in the smaller changes to velocity profile within the canopy as the approaching wind direction changed and smaller deflection angles occurring from the driving force. Correlation analysis determined that the integral length scales in the wake of the slenderer buildings are significantly larger in size, than that was seen for the low-rise buildings of the same cross section. These larger eddies result in the reduced sensitivity of the slenderer buildings to the approaching wind direction.

REFERENCES

- Castro IP, Cheng H, & Reynolds R, 2006, Turbulence over urban-type roughness: deductions from wind-tunnel measurements. *Bound.-Layer Met.*, 118, pp.109-131.
- Cheng H & Castro IP, 2002, Near Wall Flow over Urban-like Roughness. *Bound.-Layer Met.*, 104, pp. 229–259.
- Grimmond CSB & Oke TR, 1999, Aerodynamic Properties of Urban Areas Derived from Analysis of Surface Form. *J. App. Meteor. and Clim.*, 38, pp. 1262-1292.
- Kanda M, et al., 2013. A New Aerodynamic Parametrization for Real Urban Surfaces. *Bound.-Layer Met.*, 148, pp. 357-377.
- Maronga B, et al., 2015. The Parallelized Large-Eddy Simulation Model (PALM) version 4.0 for atmospheric and oceanic flows: model formulation, recent developments, and future perspectives. *Geosci. Model Dev.*, 8, pp. 2515-2551.
- Marucci D, Carpentieri M & Hayden P, 2018, On the Simulation of Thick Non-Neutral Boundary Layers for Urban Studies in a Wind Tunnel. *Int. J. Heat Fluid Flow*, 72, pp. 37-51.
- Sessa V, Xie ZT, & Herring S, 2020, Thermal Stratification Effects on Turbulence and Dispersion in Internal and External Boundary Layers. *Bound.-Layer Met.*, 176, pp. 61-83.
- Xie ZT & Castro IP, 2006, LES and RANS for turbulent flow over arrays of wall-mounted obstacles. *Flow, Turb. and Comb.*, 76, p. 291–312.
- Xie ZT, Coceal O & Castro IP, 2008, Large-Eddy Simulation of Flows over Random Urban-like Obstacles. *Bound.-Layer Met.*, 129, pp. 1-23.